

DESIGN FOR THE COLON CANCER INHIBITORS TARGETING THYMIDYLATE KINASE BY USING *INSILICO* STUDIES

MOHD ABDUL BAQI¹, KOPPULA JAYANTHI², RAMAN RAJESHKUMAR^{1*}

¹Department of Pharmaceutical Biotechnology, JSS College of Pharmacy, JSS Academy of Higher Education and Research, Ooty, Nilgiris, Tamil Nadu, India. ²Department of Pharmaceutical Chemistry, JSS College of Pharmacy, JSS Academy of Higher Education and Research, Ooty, Nilgiris, Tamil Nadu, India

*Corresponding author: Raman Rajeshkumar; *Email: bathmic@jssuni.edu.in

Received: 09 Dec 2023, Revised and Accepted: 02 Mar 2024

ABSTRACT

Objective: Thymidylate Kinase (TMK) plays a crucial role in bacterial DNA synthesis by catalyzing the phosphorylation of Deoxythymidine Monophosphate (dTMP) to form Deoxythymidine Diphosphate (dTDP). Consequently, this enzyme emerges as a promising target for developing novel anti-cancer drugs. However, no anti-cancer drugs have been reported for this target until now.

Methods: Ligands obtained from Benzylidene derivatives were examined for their potency by using molecular docking by glide module, Qikprop screening of Absorption, Distribution, Metabolism, and Excretion (ADME) study, and prime Molecular Mechanics in Generalized Bond Surface Area study (MM-GBSA) by binding free energy. Hereafter, a Molecular Dynamic (MD) simulation was performed at 100 ns to assess the stability of the potential ligand as a Human TMK (*HaTMK*) inhibitor.

Results: These ten molecules showed good binding affinity and hydrogen and hydrophobic bond interactions with Arg150, Phe42, and Phe72 in the *HaTMK* enzyme (PDB id: 1E2D). Among them, trichloro-6-(((4-hydroxyphenyl)imino)methyl)phenol molecule had a high XP-docking score of (-7.87 kcal/mol), based on extra-precision data. Prime MM-GBSA studies also showed promising binding affinities i.e., ΔBind (-34.59 kcal/mol), ΔLipo (-13.92 kcal/mol), and ΔvdW (-34.42 kcal/mol). Arg76 and Phe72 residues maintained constant interactions with the ligand during Molecular Dynamics (MD) simulation. This ligand showed a potential binding affinity for the TMK target.

Conclusion: The trichloro-6-(((4-hydroxyphenyl)imino)methyl)phenol ligand has active sites, namely benzene ring, benzylidene, and oxygen group, which actively participate in interaction with the protein of *HaTMK*, thus indicating good potential activity as the inhibitor of *HaTMK* to treat colon cancer.

Keywords: Thymidylate kinase (TMK), Molecular docking, Molecular dynamics simulations, MM-GBSA, HTVS, ADME, cancer, *HaTMK*

© 2024 The Authors. Published by Innovare Academic Sciences Pvt Ltd. This is an open access article under the CC BY license (<https://creativecommons.org/licenses/by/4.0/>)
DOI: <https://dx.doi.org/10.22159/ijap.2024v16i3.50079> Journal homepage: <https://innovareacademics.in/journals/index.php/ijap>

INTRODUCTION

Cancer is defined as the rapid proliferation of cells, which is a significant cause of death throughout the world [1]. Because of a series of multiple mutations in genes, cell functions are disrupted, leading to cancer. In the broad sense, more than 277 distinct forms of cancer are referred to as Cancer. After observing various phases of cancers, scientists have suggested that several gene mutations contribute to the aetiology of cancer. As a result of these alterations, gene anomalies in cell division occur [2]. As per the GLOBOCAN cancer statistics, it is assumed that there are nearly 20 million new cancer diagnoses, and approximately 10 million cancer-related deaths were recorded in 2020. With almost 2.3 million new cases (11.7%), female breast cancer has been recorded as the deadliest malignancy. Lung cancer (11.4%), colorectal cancer (10.0%), prostate cancer (7.3%), and stomach cancer (5.6%) have been reported to be the following most common cancers. Accounting for an anticipated 1.8 million deaths, lung cancer continued to be the most common cause of cancer-related mortality; Colorectal (9.4%), liver (8.3%), stomach (7.7%), and female breast (6.9%) cancers were the next in line [3]. Globally, colon cancer is among the most common cancers. Compared to rectal cancer, colon cancer is more common. Colon cancer has three phases. What they are is Stage I: The tumour will be in the mucosa and submucosal layer of the colon wall. Stage II: Extramural tissue will get affected by the tumour.

Stage III: In this phase, the tumour also affects regional nodes [4]. Nowadays, TMK is an attractive target because, in eukaryotic cells, it plays an important role in DNA formation. TMK is a catalyst between Deoxythymidine Monophosphate (dTMP) and Deoxythymidine Diphosphate (dTDP). In the presence of nucleoside kinase, this dTDP forms Deoxythymidine Triphosphate (dTTP) [5]. dTTP plays a pivotal role in DNA formation. When TMK is blocked, it hinders the formation of dTDP, resulting in the blockade of dTTP. As a result, DNA production is inhibited. This function has made TMK a

desirable target for developing antibiotics and anticancer drugs. TMK enzyme is present in human (eukaryotic) and bacterial (prokaryotic) cells. The eukaryotic consensus sequence Gxxx1xGKx of the p-loop contains arginine residues in its X₁ position, which interacts with Adenosine Triphosphate (ATP) [6]. The prokaryotic consensus sequence Gxxx1xGKx of the p-loop possesses glycine residues in its X₁ position. Arginine residues present in the LID region interact with ATP [7] identifying the low (19%) sequence homology between the human and *S. aureus* TMK X-ray structures adds credence to TMK's potential as a target for developing anti-cancer drugs and antibiotics. Arg76, Arg97, and Arg150 are present in the TMP binding cavity. These residues and Phe72 actively participated in transferring ATP from dTMP which results in the formation of dTDP. The possibility would be to design inhibitors containing hydrogen-bonding groups targeting Arg76, Arg97, and Arg150 at the base of the TMP-binding cavity of TMK. In the present work, we have targeted the charged residues Arg76, Arg97, and Arg150 at the base of the TMP-binding cavity and Phe72 of TMK [8]. We have designed ten ligands from benzylidene derivatives. The designed ligands are Trichloro-6-(((4-hydroxyphenyl)imino)methyl)phenol (Compound 1), 3-(((4-hydroxyphenyl)imino)methyl)-6-methoxybenzene-1,2-diol (Compound 2), 3,6-dichloro-4-(((4-hydroxyphenyl)imino)methyl)benzene-1,2-diol (Compound 3), 4-((3-fluorobenzylidene)amino)phenol (Compound 4), 3-(((4-hydroxyphenyl)imino)methyl)benzene-1,2-diol (Compound 5), 2,4-dichloro-6-(((4-hydroxyphenyl)imino)methyl)phenol (Compound 6), 2-(((4-hydroxyphenyl)imino)methyl)-6-methoxyphenol (Compound 7), 4-((3-nitrobenzylidene)amino)phenol (Compound 8), 3,6-dichloro-2-(((4-hydroxyphenyl)imino)methyl)phenol (Compound 9), 3,4-dichloro-2-(((4-hydroxyphenyl)imino)methyl)phenol (Compound 10). A Previous study reported that N-(3,4,5-trimethoxybenzylidene)-2-(5-(4-nitrophenoxy)methyl-1,3,4-oxadiazol-2-yl) thioacetohydrazide

ligand inhibits neoplastic cell growth in hepatocellular carcinoma by performing *in vitro* studies against HepG-2 cell line. This ligand has IC₅₀ value of 90.2±8.1 µg/ml, which shows moderate cytotoxicity against HepG-2 cells which is near to the reference anti-cancer drug 5-fluorouracil (5FU) [9]. This ligand also contains benzylidene moiety, but this study was not performed on colon cancer [10]. We are targeting particularly colon cancer with benzylidene derivatives. We have performed *in silico* studies; in which we obtained glide score (-7.87 kcal/mol) in XP docking, and MM-GBSA studies we obtained binding affinity (ΔBind-34.59 kcal/mol) and in MD studies this ligand showed interactions with active target Arg76, Phe72. Similarly, we performed *in silico* studies for the standard drug doxycycline for which we obtained glide score (-8.07 kcal/mol) and binding affinity (ΔBind-52.60 kcal/mol). When we compared the *in silico* results of doxycycline with Compound 1, benzylidene derivatives showed good glide score and binding affinity near to reference standard drug doxycycline whereas PDB id 1E2D co-crystal ligand showed less glide score (-6.61 kcal/mol) and binding affinity (ΔBind-33.50 kcal/mol) compared to benzylidene derivatives. This ligand may give promising results in *in vitro* activity against colon cancer.

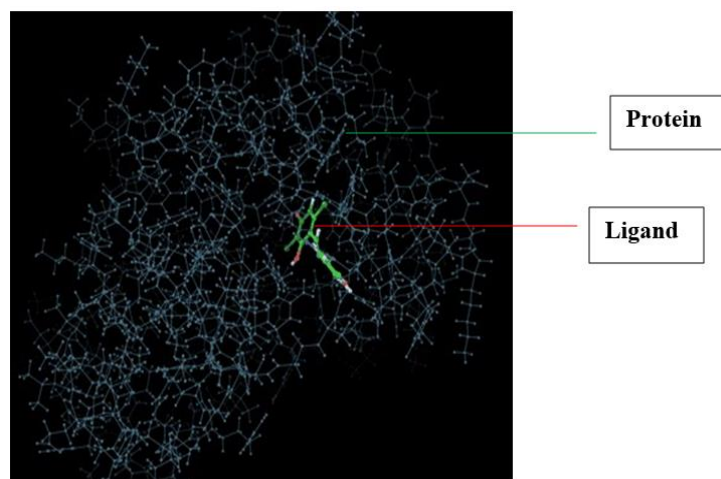


Fig. 1: Compound 1 protein-ligand interaction complex (PDB id: 1E2D) in molecular docking

Binding free energy calculations using prime MM-GBSA

The binding free energy for each protein-ligand combination was calculated using the prime MM-GBSA approach (Schrödinger suite 2021-4). An OPLS3e force field with a VSGB 2.0 solvation model was used for energy minimization [16]. This technique contains optimal implicit solvation for hydrogen bonding, self-contact interactions, and hydrophobic interactions, in addition to a physics-based correction [17].

Study of molecular dynamics simulations

Time-step methods were used in the reference system propagator algorithm for bonded Electrostatic forces, which can be non-bonded, short-range, or long-range. Every 100 PS, data was collected [18] and trajectories were analyzed. We have performed MD simulation using (Schrödinger suite 2021-4), to investigate top-ranked compounds' nuclear binding behaviour, and understand molecular interfaces [19]. To solve the complex Compound 1/1E2D, the TIP4P water model with orthorhombic periodic borders and a buffer zone of 10 between Protein atoms and box edges was employed [20]. To neutralize the generated system 0.15 molar, NaCl counter ions were provided. The energy was minimized using the OPLS4 force field adjustments. Long-range electrostatic interactions were calculated with a tolerance of 1e-09 utilizing the Ewald Smooth Particle Mesh method [21]. The

MATERIAL AND METHODS

Molecular docking

Energy, score, and e-model values determined the optimal docked attitude for every ligand. A computer technology known as molecular docking has been utilized for predicting the ligand's binding mechanism and affinity for the target [11]. The docked conformers were tuned depending on the system's total energy [12]. The X-ray crystal structure of *human TMK* (PDB id 1E2D, resolution: 1.65 Å) was chosen for the modeling effort. Schrödinger suite 2021-4, preparation of the Wizard module was used to prepare the protein [13]. The addition of hydrogen destroyed the crystallographic water molecules [14]. Prime (Schrödinger suite 2021-4) accommodated the missing side chain. The OPLS3e forcefield was employed to reduce energy consumption while maintaining heavy atoms Root Mean Square Deviations (RMSD) at 0.30 [15]. The active site was characterized by a radius of ten around the bound ligand in a grid box with the co-crystallized ligand in the middle. Glide was used to dock the 10 ligands synthesized with LigPrep in extra-precision (XP) mode, with all other settings left at their default. Glide energy, score, and e-model values determined the optimal docked attitude for every ligand. In fig. 1, we can see the protein-ligand complex.

short-range Vander Waals and Coulomb interactions were estimated at a cut-off radius of 9.0. One hundred ns of MD simulations at two fs per time step were done at 300 Kelvin and 1 bar of pressure in an isothermal-isobaric ensemble [Simulation of a system with constant number (N) and constant temperature (T), but variable pressure (P)]. At 100 and 200 PS, The Nose-Hoover thermostat chain thermostat and Martyna-Tobias-Klein barostat techniques are integrated [22]. Multiple time-step methods were used in the reference system propagator algorithm for bonded Electrostatic forces, which can be non-bonded, short-range, or long-range. Every 100 PS, data was collected, and trajectories were analyzed [23] to solve the complex compound 1/1E2D as shown in fig. 2.

RESULTS

Binding free energy calculations and molecular docking

Using TMK (PDB id: 1E2D), Schrodinger Suite 2021-4 validates docking studies using the ligand-based virtual screening technique. The bound ligands' conformational orientation was identical with accuracy to the co-crystal of RMSD (1.6 Å) using docking protocol. This docking used a virtual screening approach to remove the functional groups that reacted with ligands using Lipinski's rule-XP-docking results in glide score, emodel, evdw, ecol, and energy.

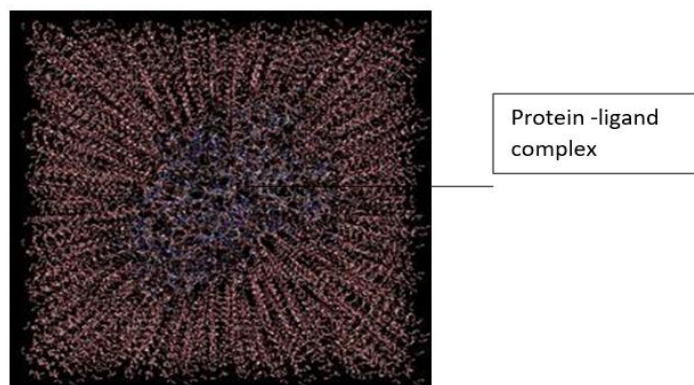


Fig. 2: Protein-ligand complex compound 1/1E2D in dynamics simulation

Table 1: The XP-docking score of compounds 1-10 in the catalytic pocket of (PDB id: 1E2D) thymidylate kinase (kcal/mol)

Compound code	^a gscore	^b gemodel	^c gevdw	^d gecoul	^e genergy
1	-7.872	-42.314	-29.514	-6.712	-36.227
2	-7.437	-57.574	-29.168	-13.476	-42.645
3	-7.336	-48.039	-31.086	-13.773	-44.859
4	-7.252	-54.498	-30.501	-11.242	-41.743
5	-6.871	-49.647	-29.114	-6.021	-35.135
6	-6.864	-43.256	-31.556	-8.065	-39.621
7	-6.772	-48.786	-30.856	-5.584	-36.440
8	-6.727	-48.286	-30.408	-5.437	-35.846
9	-6.716	-43.583	-33.454	-5.275	-38.729
10	-6.671	-40.648	-27.579	-6.798	-34.377

^aglide score, ^bglide model energy, ^cglide van der Waals energy, ^dglide Coulomb energy, ^eglide energy.

The docking results in table 1 show that all ligands have at least one hydrogen bond with amino acids, and the glide scores range from -7.87 to -6.67 kcal/mol. In the XP-docking, compound 1 and compound 2 showed high glide scores of -7.87 and -7.43 kcal/mol respectively, and

the compounds, compound 3 and compound 4 also showed good glide scores of -7.33 and -7.25 kcal/mol respectively. After docking, minimized binding free energies (ΔG_{Bind}) of the selected hits top-scoring poses increased from -34.59 to -58.71 kcal/mol.

Table 2: Contribution of binding free energy (MM-GBSA) (kcal/mol) between compounds 1-10 (PDB id: 1E2D) thymidylate kinase complexes

Compound code	^a ΔG_{Bind}	^b ΔG_{Coul}	^c ΔG_{HB}	^d ΔG_{Lip}	^e ΔG_{vdW}
1	-34.594	-117.005	-1.010	-13.921	-34.428
2	-50.883	62.091	2.694	-24.864	-46.317
3	-47.213	0.254	1.966	-23.828	-44.419
4	-52.108	3.607	-0.355	-19.795	-52.524
5	-46.339	61.322	2.794	-17.573	-33.748
6	-58.715	-2.647	2.020	-24.991	-38.999
7	-41.428	-13.320	2.212	-21.822	-43.949
8	-39.493	6.460	2.270	-20.293	-40.289
9	-34.862	18.906	4.655	-22.138	-43.1902
10	-35.867	16.016	4.905	-23.623	-35.675

^afree energy of binding, ^bCoulomb energy, ^chydrogen bonding energy, ^dhydrophobic energy (non-polar contribution estimated by solvent accessible surface area), ^evan der Waals energy.

Table 3: The number of hydrogen bonds and intermingling amino acid residues for the ten hits in the Thymidylate kinase catalytic pocket (PDB id: 1E2D)

Compound code	Number of hydrogen bonds	Interacting amino acid residues
1	2	PHE42, ARG150
2	4	ASP15, ARG150, TYR98, ARG76
3	3	ASP15, TYR98, ARG76
4	2	ARG76, GLU152
5	3	GLU152, PHE42, ARG76
6	2	GLU152, PHE42
7	2	GLU152, PHE42
8	1	GLU152
9	1	GLU152
10	2	GLU152, PHE42

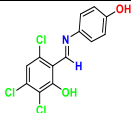
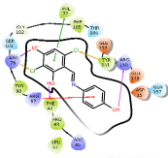
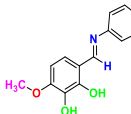
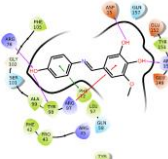
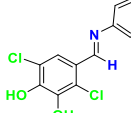

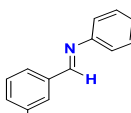
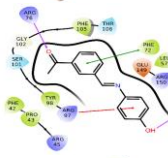
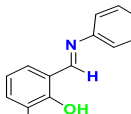

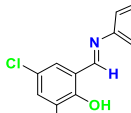
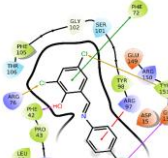
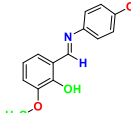
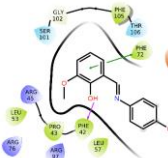
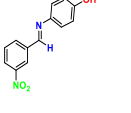
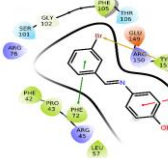
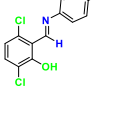
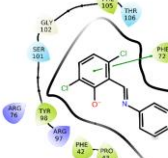
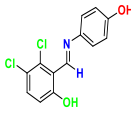
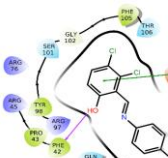
Compound code	Structure	2D Interaction	Glide score (kcal/mol)
1			-7.872
2			-7.437
3			-7.336
4			-7.252
5			-6.871
6			-6.864
7			-6.772
8			-6.727
9			-6.716
10			-6.671

Fig. 3: 2D interaction diagrams of the ten chemicals in the thymidylate kinase catalytic pocket (PDB id: 1E2D), Depicts the all-molecule hits 2D interactions. Compound 1 has a gliding score of -7.87 kcal/mol and a binding affinity of -34.59 kcal/mol

In table 2, the considerable Van der Waal energy (ΔG_{VdW}) ranges from -33.74 to -52.52 kcal/mol, and the moderately preferred hydrophobic (ΔG_{Lip}) ranges from -13.92 to -24.99 kcal/mol, which favors total binding energy. Compound 1 got the most excellent glide scores compared with other compounds. Compound 1 glide score was -7.87 kcal/mol. Compound 6 and compound 4 showed the highest binding affinity with -58.71 kcal/mol and -52.10 kcal/mol, respectively; the compound 1 binding affinity was -34.59 kcal/mol, respectively, according to the critical free energy calculation MM-GBSA method. Compounds 2D interactions are depicted in fig. 3.

Table 3 shows hydrogen bonding interactions with amino acid residues for designed molecules. The compound 1 amino acid

interactions are with contacts Arg150, Tyr151, Phe42, Arg97, Arg76, Phe72. Compound 1 showed hydrogen bond interactions with Phe42, Arg150, and amino acid residues. It was chosen for further investigation by considering both docking and binding affinity scores. Compound 1, compound 2, compound 3, compound 4, and compound 6 showed promising results compared to other compounds. The results above show that the compound 1 glide score is higher than that of other compounds, co-crystal ligand, and standard drug doxycycline. This result is depicted in fig. 4. Considering the glide score, we have proceeded with further study. As a result, we underwent deep investigation by performing md simulation study for compound 1.

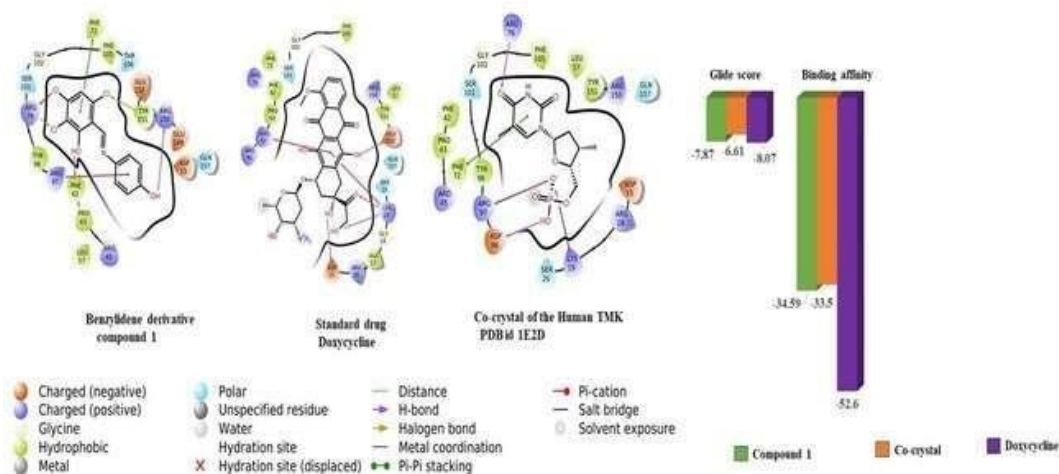


Fig. 4: Comparison of glide score and binding affinity between compound 1, doxycycline, and Co-crystal

MD simulation study

The ligand trichloro-6-((4-hydroxyphenyl) imino) methyl phenol compound 1/1E2D docked pose was ran for 100 ns in molecular dynamic simulations. By doing this study, we observed results in RMSD; root mean square fluctuations (RMSF) protein-ligand interactions fractions, protein-ligand contacts timeline, and protein-ligand contacts with a 2D diagram. $C\alpha$ atom (lig) fit on prot was observed and stabilized simulations docked pose for ligand compound 1/1E2D in RMSD was evaluated. The value of the $C\alpha$ atom was 0.8 to 3.1 Å and the (lig) fit prot was 0.5 to 3.2 Å. The $C\alpha$ atom for the ligand maintained stability for 65 ns out of 100 ns, and for the remaining 35 ns $C\alpha$ atom maintained moderate stability out of 100 ns. The ligand was stable from 0.9 to 1.3 Å, which is 15 ns to 50 ns and the next phase of stability starts from 1.2 to 3.1 Å i.e., 70

ns to 100 ns ligand was stable in the protein. The moderate stability for the ligand starts from 0.8 to 1.2 Å i.e., 0 to 15 ns ligand showed moderate fluctuations. The next phase of moderate stability starts from 1.1 to 1.6 Å i.e., 50 to 70 ns ligand showed moderate fluctuations.

(lig) fit prot for the ligand maintained stability for 72 ns out of 100 ns, and for the remaining 28 ns (lig) fit prot maintained moderate stability out of 100 ns. From 0.4 to 0.8 Å i.e., 18 ns to 55 ns ligand was stable and the next phase of stability starts from 1.1 to 3.2 Å i.e., 65 ns to 100 ns ligand was steady in the protein. The moderate stability for the ligand starts from 0.5 to 1.6 Å i.e., 0 to 18 ns ligand showed moderate fluctuations. The next phase of moderate stability starts from 0.8 to 1.4 Å i.e., 55 to 65 ns ligand showed moderate fluctuations. These results are depicted in fig. 5.

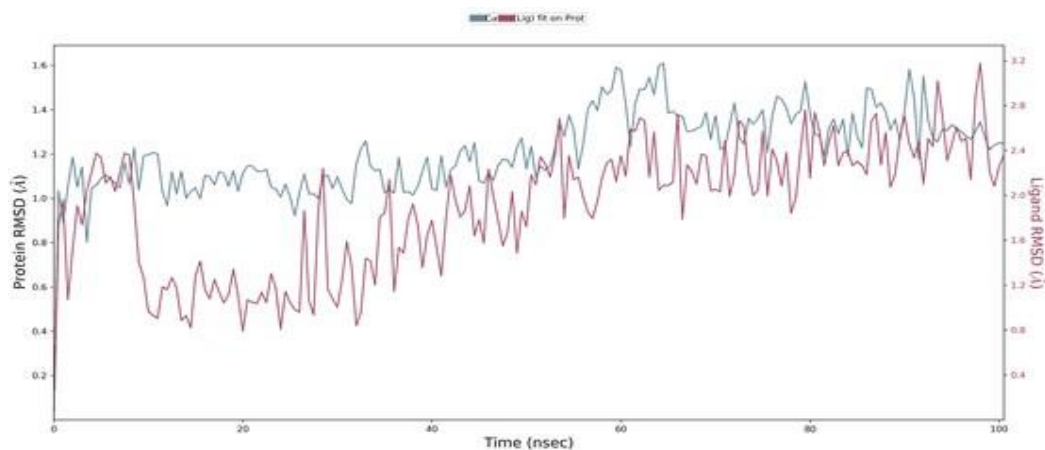


Fig. 5: RMSD graph for compound 1/E2D complex. RMSD-root mean square deviations

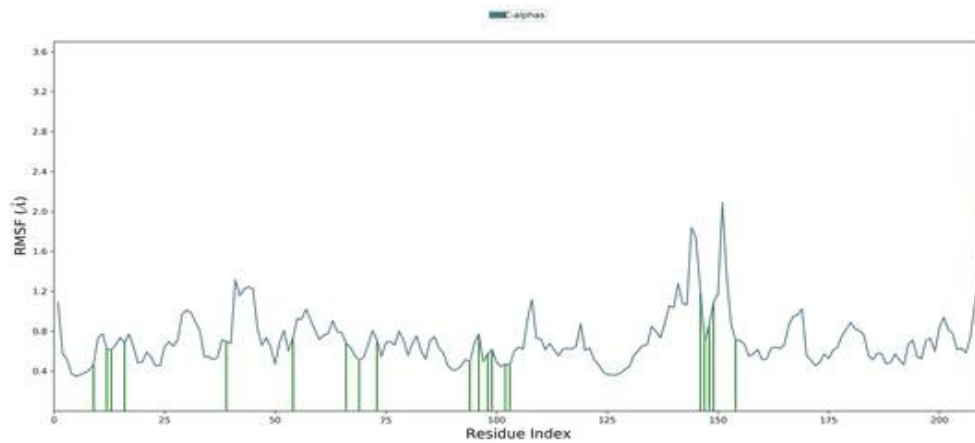


Fig. 6: RMSF diagram for compound 1/1E2D complex. RMSF-root mean square fluctuations

In the RMSF, we observed there are no significant fluctuations. The C α atom showed initial fluctuations from 0.4 to 2.0 Å, as depicted in fig. 6, and maintained the overall simulations. Ligands with particular changes with amino acids were observed, and maximum fluctuations were observed at 145 to 155 ns and 40 to 55 ns, amino acids RMSF values were 0.5 to 2.0 Å, and 0.5 to 1.2 Å, respectively. We observed minimum fluctuations of 10 to 15 ns, 60 to 75 ns, and 90 to 105 ns, with amino acids RMSF values at 0.4 to 0.8 Å, 0.6 to 1.0 Å, and 0.4 to 0.6 Å, respectively.

In fig. 7, the ligand maintained continuous interactions with amino acids with different bonds like water bridge, hydrogen bonds, and

ionic and hydrophobic interactions, respectively, and this ligand also formed multiple interactions with amino acids. The ligand formed contacts with amino acids. Ligand formed a water bridge bond with Glu12, His69, and Ala99 residues and maintained it at 0.2% out of 1.3%. This ligand formed hydrophobic interactions with Lys19, Leu57, Phe72, Phe105, and maintained its interactions at 0.8% out of 1.3%, and hydrogen bond interactions were formed with Tyr106, Arg76, amino acids, and maintained its interactions at 1.1% out of 1.3%, and ionic interaction with Arg16 residue and this ligand formed multiple interactions with amino acids Asp15, Phe42, Arg76, Arg97, Ser101, Gly102, Glu149, Arg150, Tyr151, Glu152, Gln157, maintaining the multiple interactions percentage at 1.2% out of 1.3%.

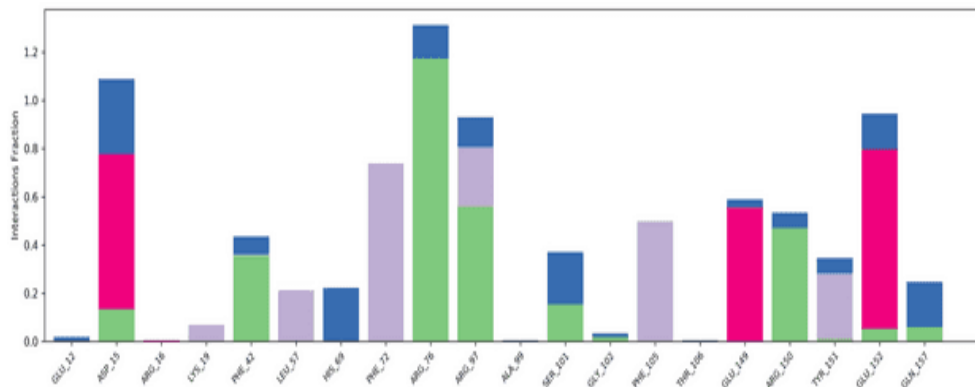


Fig. 7: Protein-ligand contacts profile for compound 1/1E2D complex

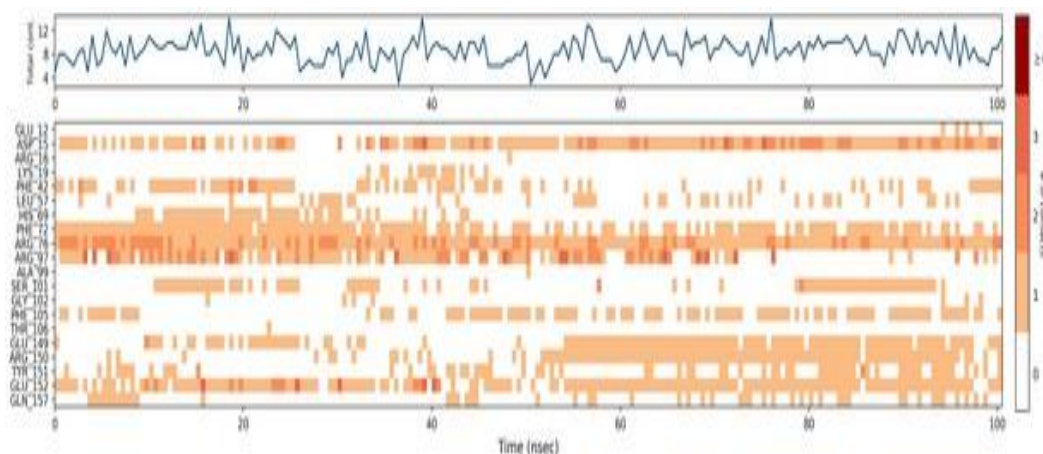


Fig. 8: Timeline representation for compound 1/1E2D complex

In fig. 8, it shows that Arg76, Phe72, and Glu152 are particular amino acids that continuously interact with ligand throughout 100 ns. Asp15 maintained constant contact with ligand from 0 to 30 ns, and 35 to 100 ns. Phe42 maintained continuous contact with ligand from 0 to 27 ns, 35 to 58 ns, and 62 to 100 ns. Arg97 maintained continuous contact with ligand from 0 to 70 ns. Ser101 maintained constant contact with ligand from 10 to 40 ns and 75 to 100 ns.

Phe105 maintained continuous contact with ligand from 0 to 10 ns and 30 to 100 ns. Glu149 maintained constant contact with ligand from 10 to 35 ns and 55 to 100 ns. Arg150 maintained continuous contact with ligand from 50 to 100 ns in overall 100 ns of simulations. Finally, Glu152, Phe72, and Arg76 maintained the interactions with ligand throughout 100 ns of simulations. Protein-ligand contacts present within the 2D diagram are shown in fig. 9.

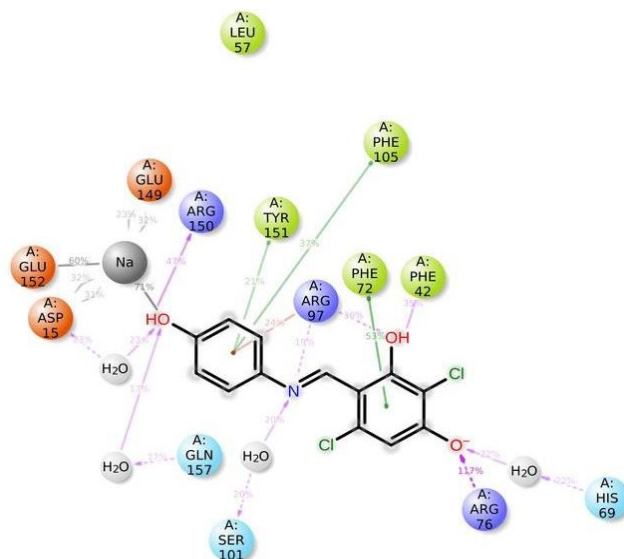


Fig. 9: 2D diagram for compound 1/1E2D complex

Phe72 maintained continuous contact with the aromatic ring with pi-pi stacking; the bond was stable at 53%. Arg76 maintained constant contact with the oxygen group with a hydrogen bond, the bond was steady at 117%. Arg150 maintained continuous contact with the hydroxy group with a hydrogen bond, the bond was stable at 47%. Phe105 maintained constant contact with benzene by forming pi-pi stacking; the bond was steady at 47%. Phe42 maintained continuous contact with the hydroxy group by forming a hydrogen bond, the bond was stable at 35%. His69 maintained constant contact with the oxygen group by forming a hydrogen bond, the bond was stable at 22%. Arg97 maintained continuous contact with the nitrogen group on the (benzylidene moiety) by forming a hydrogen bond, the bond was stable at 19%. Ser101 maintained constant contact with the nitrogen group on the (benzylidene moiety) by forming a hydrogen bond, the bond was stable at 20%. Arg97 maintained continuous contact with the benzene with an ionic bond, the bond was stable at 24%. Phe105 maintained constant contact with the aromatic ring by forming pi-pi stacking, the bond was steady at 37%. Tyr151 maintained continuous contact with the aromatic ring by forming pi-pi stacking, the bond was steady at 21%. Glu152 maintained constant contact with the hydroxy group by forming a water bridge, and the bond was steady at 60%. Asp15 maintained continuous contact with the hydroxy group with the water bridge, the bond was stable at 23%. As per the above results, the ligand compound 1 showed promising activity in developing the new anticancer agents.

DISCUSSION

Previous studies have identified pyridine-fused and arene-fused isothiazolone analogues as inhibitors targeting the *HaTMK* enzyme, crucial for developing new cancer treatments. The pyridine-fused isothiazolone analogue exhibits a strong affinity for the B-site of *HaTMK*, with a binding affinity of 39.8 kcal/mol. This analogue engages with the LID region, forming hydrogen bonds with Ala145 and Glu149's amide nitrogen atoms. Additionally, a hydrophobic pocket formed by residues Ala141, Ala145, Ala140, Leu137, Leu135, Ala17, and Val14 envelops the analogue. MD simulations demonstrated its stability for 35 ns out of a 100 ns simulation, maintaining a backbone atom RMSD below 2.5 Å. The arene-fused

isothiazolone analogue binds to both the B-site and D-site of *HaTMK*, showing binding affinities of 16.2 kcal/mol and 23.3 kcal/mol, respectively [24]. In contrast, the benzylidene amino phenol derivative exhibits a higher binding affinity of 34.59 kcal/mol at the same *HaTMK* complex site. Benzylidene amino phenol derivative remained stable for 65 ns in a 100 ns MD simulation, with a backbone atom RMSD below 3.1 Å. This derivative also interacts with the LID region, forming hydrogen bonds with Phe42 and Arg150, while a hydrophobic pocket surrounds it, formed by Lys19, Leu57, Phe72, and Phe105. In another study, benzylidene moiety showed an IC₅₀ value of 90.2±8.1 µg/ml against hepatocellular cancer cells in *in vitro*, similar promising results are anticipated against colon cancer [9]. Moreover, *HaTMK* has been targeted in studies related to the monkeypox virus. The compound DB16335, with a glide score of -9.7 kcal/mol and binding affinities of 60.07 kcal/mol and 16.06 kcal/mol from MM-GBSA and Molecular Mechanics Poisson-Boltzmann Surface Area method (MM-PBSA) assays, respectively, demonstrated stability over 75 ns of a 300 ns MD simulation. It maintained a backbone atom RMSD of 2.0 Å and interacted with residues including Asp13, Thr18, and Arg41, forming hydrogen bonds with Phe38, and Glu142, among others, effectively inhibiting the monkeypox virus [25]. These findings underscore the potential of the benzylidene amino phenol derivative as a potent inhibitor of *HaTMK*, similar to the efficacy observed in the monkeypox study, thus highlighting its promise for colon cancer treatment through *HaTMK* inhibition.

CONCLUSION

Based on these findings, benzylidene amino phenol derivatives have emerged as highly promising candidates for anti-colon cancer drugs. Notably, the compound 1-trichloro-6-((4-hydroxyphenyl)imino)methylphenol demonstrated significant potential with an impressive glide score of -7.87 kcal/mol and a binding affinity (Δ Bind) of 34.59 kcal/mol. MD studies revealed that this compound remained stable for 65 ns during a 100 ns simulation, with a backbone atom RMSD stability of 3.1 Å. The interaction between Arg97 and the benzylidene active moiety of the compound was particularly noteworthy. Additionally, the amino acids Arg76, Phe72, and Glu152 maintained continuous contact with the

compound, suggesting that benzylidene amino phenol derivatives can inhibit the *HaTMK* enzyme, thereby offering a potential treatment for cancer. Previous studies have shown that pyridine-fused and arene-fused isothiazolone analogues, which target the same *HaTMK*, exhibited lower binding affinities compared to our benzylidene amino phenol derivatives. Furthermore, benzylidene moiety derivatives have been reported to inhibit hepatocellular cancer cells with an IC50 value of 90.2±8.1 µg/ml in *in vitro*. Based on these results, we anticipate that our derivatives will also show promising *in vitro* results against colon cancer. Our future plans include targeting colon cancer through formulation studies and positioning benzylidene amino phenol derivatives as leading candidates for the development of anti-colon cancer drugs. However, further experimental *in vivo* studies are necessary to confirm their therapeutic efficacy and safety.

ACKNOWLEDGMENT

The authors would like to thank the Department of Pharmaceutical Biotechnology and Department of Pharmaceutical Chemistry, JSS College of Pharmacy, Ooty, Tamil Nadu, for providing facilities for conducting Research.

FUNDING

No funding was received for this work

AUTHORS CONTRIBUTIONS

Mohd Abdul Baqi-Conceptualization, validation, writing-original draft preparation and Data curation. Koppula Jayanthi-Data curation, methodology, writing-Review and Editing. Raman Rajeshkumar-Conceptualization, Formal analysis, validation, and supervision.

CONFLICT OF INTERESTS

Declared none

REFERENCES

- Shewach DS, Kuchta RD. Introduction to cancer chemotherapeutics. *Chem Rev*. 2009 Jul 8;109(7):2859-61. doi: 10.1021/cr900208x, PMID 19583428.
- Hassanpour SH, Dehghani M. Review of cancer from the perspective of molecular. *J Cancer Res Pract*. 2017;4(4):127-9. doi: 10.1016/j.jcrpr.2017.07.001.
- Sung H, Ferlay J, Siegel RL, Laversanne M, Soerjomataram I, Jemal A. Global cancer statistics 2020: GLOBOCAN estimates of incidence and mortality worldwide for 36 cancers in 185 countries. *CA Cancer J Clin*. 2021 May;71(3):209-49. doi: 10.3322/caac.21660, PMID 33538338.
- Labianca R, Beretta G, Gatta G, de Braud F, Wils J. Colon cancer. *Crit Rev Oncol Hematol*. 2004;51(2):145-70. doi: 10.1016/j.critrevonc.2004.03.003, PMID 15276177.
- Munier Lehmann H, Chaffotte A, Pochet S, Labesse G. Thymidylate kinase of mycobacterium tuberculosis: a chimera sharing properties common to eukaryotic and bacterial enzymes. *Protein Sci*. 2001 Jun;10(6):1195-205. doi: 10.1110/ps.45701, PMID 11369858.
- Ostermann N, Schlichting I, Brundiers R, Konrad M, Reinstein J, Veit T. Insights into the phosphoryl transfer mechanism of human thymidylate kinase gained from crystal structures of enzyme complexes along the reaction coordinate. *Structure*. 2000;8(6):629-42. doi: 10.1016/s0969-2126(00)00149-0, PMID 10873853.
- Kotaka M, Dhaliwal B, Ren J, Nichols CE, Angell R, Lockyer M. Structures of *S. aureus* thymidylate kinase reveal an atypical active site configuration and an intermediate conformational state upon substrate binding. *Protein Sci*. 2006;15(4):774-84. doi: 10.1110/ps.052002406, PMID 16522804.
- Ostermann N, Schlichting I, Brundiers R, Konrad M, Reinstein J, Veit T. Insights into the phosphoryltransfer mechanism of human thymidylate kinase gained from crystal structures of enzyme complexes along the reaction coordinate. *Structure*. 2000;8(6):629-42. doi: 10.1016/s0969-2126(00)00149-0, PMID 10873853.
- Lingaraju S, Venkatesh L. Effect of 2 w yoga and meditation on emotional quotient. *Natl J Physiol Pharm Pharmacol*. 2018;8(9):1269-70. doi: 10.5455/njppp.2018.8.0416408052018.
- Blanco Jerez LM, Rangel Oyervides LD, Gomez A, Jimenez Perez VM, Munoz Flores BM. Electrochemical metallization with Sn of (E)-4-((4-nitrobenzylidene) amino)phenol in non-aqueous media: characterization and biological activity of the organotin compound. *Int J Electrochem Sci*. 2016;11(1):45-53. doi: 10.1016/S1452-3981(23)15825-1.
- James JP, Aiswarya TC, Priya S, Jyothi D, Dixit SR. Structure-based multitargeted molecular docking analysis of pyrazole-condensed heterocyclics against lung cancer. *Int J App Pharm*. 2021;3(6):157-69. doi: 10.22159/ijap.2021v13i6.42801.
- Dar AM, Mir S. Molecular docking: approaches, types, applications and basic challenges. *J Anal Bioanal Tech*. 2017;8(2):1-3. doi: 10.4172/2155-9872.1000356.
- Sastry GM, Adzhigirey M, Day T, Annabhimoju R, Sherman W. Protein and ligand preparation: parameters, protocols, and influence on virtual screening enrichments. *J Comput Aided Mol Des*. 2013 Mar;27(3):221-34. doi: 10.1007/s10822-013-9644-8, PMID 23579614.
- Sukumaran S, MM, SS, BA, SS S ST. In silico analysis of acridone against TNF-α and PDE4 targets for the treatment of psoriasis. *Int J Res Pharm Sci*. 2020 Dec 18;11(4):7790-8.
- Dunkel M, Fullbeck M, Neumann S, Preissner R. Super natural: a searchable database of available natural compounds. *Nucleic Acids Res*. 2006;34:D678-83. doi: 10.1093/nar/gkj132, PMID 16381957.
- Jacobson MP, Pincus DL, Rapp CS, Day T, Honig B, Shaw DE. A hierarchical approach to all-atom protein loop prediction. *Proteins*. 2004 May;55(2):351-67. doi: 10.1002/prot.10613, PMID 15048827.
- Dhawale S, Gawale S, Jadhav A, Gethe K, Raut P, Hiwarale N. *In silico* approach targeting polyphenol as Fabh inhibitor in bacterial infection. *Int J Pharm Pharm Sci*. 2022;14(11):25-30. doi: 10.22159/ijpps.2022v14i11.45816.
- Martyna GJ, Tuckerman ME, Tobias DJ, Klein ML. Explicit reversible integrators for extended systems dynamics. *Mol Phys*. 1996;87(5):1117-57. doi: 10.1080/00268979600100761.
- Guo Z, Mohanty U, Noehre J, Sawyer TK, Sherman W, Krilov G. Probing the α-helical structural stability of stapled p53 peptides: molecular dynamics simulations and analysis. *Chem Biol Drug Des*. 2010 Apr;75(4):348-59. doi: 10.1111/j.1747-0285.2010.00951.x, PMID 20331649.
- Essmann U, Perera L, Berkowitz ML, Darden T, Lee H, Pedersen LG. A smooth particle mesh Ewald method. *J Chem Phys*. 1995;103(19):8577-93. doi: 10.1063/1.470117.
- Harder E, Damm W, Maple J, Wu C, Reboul M, Xiang JY. OPLS3: a force field providing broad coverage of drug-like small molecules and proteins. *J Chem Theory Comput*. 2016 Jan 12;12(1):281-96. doi: 10.1021/acs.jctc.5b00864, PMID 26584231.
- Martyna GJ, Tobias DJ, Klein ML. Constant pressure molecular dynamics algorithms. *J Chem Phys*. 1994 Sep 1;101(5):4177-89. doi: 10.1063/1.467468.
- Badavath VN, Sinha BN, Jayaprakash V. Design, *in silico* docking and predictive ADME properties of novel pyrazoline derivatives with selective human MAO inhibitory activity. *Int J Pharm Pharm Sci*. 2015;7:277-82.
- Chen YH, Hsu HY, Yeh MT, Chen CC, Huang CY, Chung YH. Chemical inhibition of human thymidylate kinase and structural insights into the phosphate binding loop and ligand-induced degradation. *J Med Chem*. 2016;59(21):9906-18. doi: 10.1021/acs.jmedchem.6b01280, PMID 27748121.
- Ajmal A, Mahmood A, Hayat C, Hakami MA, Alotaibi BS, Umair M. Computer-assisted drug repurposing for thymidylate kinase drug target in monkeypox virus. *Front Cell Infect Microbiol*. 2023;13:1159389. doi: 10.3389/fcimb.2023.1159389, PMID 37313340.